

Disappearance and Survival of Superconductivity in FeSe under High Pressure

Kiyotaka MIYOSHI^{1,2}, Shota YAMAMOTO¹, Atsushi SHIOTA¹, Takuya MATSUOKA¹, Masaki OHE¹,
Yumi YAMAMOTO¹ and Shijo NISHIGORI³
¹*Department of Physics and Materials Science,
Shimane University, Matsue 690-8504, Japan*

²*Next Generation TATARA Co-Creation Centre,
Shimane University, Matsue 690-8504, Japan
and*

³*Department of Materials Analysis, CIRS, Shimane University, Matsue 690-8504, Japan
(Dated: November 22, 2021)*

Superconductivity in FeSe was investigated under high pressure through the measurements of DC magnetization by using a diamond anvil cell. We successfully observed that the disappearance of the superconductivity as a results of the appearance of the non-superconducting ortho II phase above ~ 7 GPa (~ 5 GPa), when Ar (glycerin) is used as the pressure transmitting media. Contrary to this, it has been found that the superconductivity even survives under pressure above 7 GPa, when the thickness (t) of a platelet-single crystal specimen is reduced. The survival of the superconductivity above 7 GPa is consistent with a previous observation under hydrostatic pressure by using a cubic anvil apparatus, suggesting that the hydrostaticity of the pressure is improved by reducing t . It is also inferred that the appearance of the ortho II phase is due to uniaxial stress along the [001] direction.

PACS numbers:

Since the discovery of superconductivity in $\text{LaFeAsO}_{1-x}\text{F}_x$ ¹, intensive studies over the past decade have uncovered a wide variety of iron-pnictide superconductors and common unconventional superconductivity emerged from the competition with the antiferromagnetic (AFM) phase and electronic nematic phase with an orthorhombic structure, which is inferred from the characteristic phase diagrams. In early studies, a typical phase diagram for AFe_2As_2 ($A=\text{Sr}, \text{Ba}, \text{Ca}, \text{Eu}$) has been established, where a superconducting dome appears with disappearance of both AFM and nematic phases by tuning carrier doping²⁻⁵ or applying external pressure⁶⁻¹². In addition to a similar competition between the superconductivity and AFM (orthorhombic) phase in $\text{LaFeAsO}_{1-x}\text{F}_x$ ¹³, the coexistence of superconductivity with these phases has been found for $\text{NaFe}_{1-x}\text{A}_x\text{As}$ ($A=\text{Co}$ ^{14,15}, Cu ¹⁶) and SrVO_3FeAs ^{17,18}. In addition, a twin-dome structure and plateau-like single-dome structure with bipartite parent phases were found in $\text{RFeAsO}_{1-x}\text{H}_x$ with $\text{R}=\text{La}$ ¹⁹ and Sm ²⁰, respectively. In comparison, $\text{LaFeAs}_{1-x}\text{P}_x\text{O}$ was found to exhibit two superconducting domes separated by an AFM phase²¹⁻²³, suggesting that a different superconducting state is realized in each dome. To establish the phase diagram for various iron-pnictide superconductors is crucial to throw further light on the superconducting mechanism, because certain fluctuations arising from the ordered states that are either competing or coexisting with the superconductivity in the phase diagram are promising candidates for paring glue.

One of the most attractive subjects to explore the temperature (T)-pressure (P) phase diagram is FeSe. This is because the superconducting transition temperature T_c of FeSe was found to be highly enhanced in

early studies²⁴⁻²⁸. Furthermore, the nematic state was observed to appear without accompanying AFM order at ambient pressure, suggesting that FeSe provides an interesting test ground for examining the competition and coexistence of the superconducting, AFM, and nematic phases. Indeed, the disappearance of the nematic transition and a three-step increase in T_c under pressure was reported.²⁹ However, more intensive studies under pressure succeeded in elucidating the T - P phase diagram since single crystal growth to obtain purely tetragonal FeSe without mixing of hexagonal phase was enabled^{30,31}. A pressure induced AFM phase above 1.2 GPa has been shown to exist³² and a T - P phase diagram where a dome-shaped AFM phase competes with two other phases has been reported.³³ The AFM ordering was shown to be of the stripe-type through NMR³⁴ and μSR ³⁵ measurements and also to merge with the structural (nematic) transition above 1.7 GPa.³⁶ This suggests that the AFM and nematicity are strongly coupled with each other in FeSe under pressure, similar to other iron-based superconductors.

An important feature of the T - P phase diagram, which was determined by the measurements of electrical resistivity and AC susceptibility using a cubic anvil apparatus (CAA), is that T_c is significantly enhanced and reaches a maximum of ~ 37 K at ~ 6 GPa, above which the AFM phase boundary line is suddenly terminated, demonstrating the competing nature of the AFM and superconducting phases.³³ In addition, recent X-ray diffraction (XRD) measurements detected a mixing of an orthorhombic $Pnma$ phase with MnP-type structure (ortho II) above 6 GPa, which is non-superconducting and characterized by a three-dimensional network of face sharing FeSe_6 octahedra, with a superconducting orthorhombic

Cmma phase (ortho I).³⁷ A similar transition to the ortho II phase was also observed through measurements of XRD³⁸ and X-ray absorption spectroscopy³⁹. FeSe was known to undergo a structural transition at high pressure before the synthesis of purely tetragonal FeSe is possible.^{25–27,40} Although the superconductivity would be expected to disappear as the result of the appearance of the ortho II phase, no signature of the disappearance was inconsistently observed in AC susceptibility measurements using a CAA up to ~ 9 GPa.³³ It is important to clarify the origin of the inconsistency to gain more insight into the superconductivity of FeSe and also for further investigations under pressure. The origin is likely to be attributable to the difference in the hydrostaticity of the pressure cell, considering that diamond anvil cells (DACs) were commonly used for the observation of the ortho II phase.^{37–39}

In the present work, we performed DC magnetization measurements under pressure for single crystals of FeSe using DAC and Ar as the pressure-transmitting medium (PTM) and investigated the pressure variation of the superconducting volume fraction. We successfully observed that the superconductivity disappears and survives under pressure above 7 GPa depending on the thickness of the platelet single-crystal specimen used for the measurements. The superconductivity was similarly observed to disappear at lower pressure of ~ 5 GPa when less hydrostatic PTM (glycerin) was used, suggesting that uniaxial compression along the [001] direction promotes the transition into the ortho II phase.

Single-crystal specimens were obtained by a chemical vapor transport method,^{30,31} details of which are available in the literature.⁴¹ The XRD pattern of the FeSe single crystals is shown in Fig. 1(a), where the (00 l) peaks are observed, indicating that the (00 l) plane is exposed on the surface of the platelet crystals shown in the inset of Fig. 1(b). Figure 1(b) and 1(c) show the temperature (T) dependences of the DC magnetization (M) and electrical resistivity (ρ), respectively. These data indicate that T_c is ~ 9 K and the nematic transition temperature T_s is ~ 90 K at ambient pressure, both of which are consistent with those in earlier reports.^{31,33} High-pressure magnetic measurements were done by using a miniature DAC,⁴² which was combined with a sample rod of a commercial SQUID magnetometer. We used a CuBe gasket with a 0.3 mm ϕ gasket hole, where a platelet FeSe single crystal was loaded parallel to the culet plane of the diamond anvil together with a small piece of high-purity Pb to realize the in-situ determination of pressure. The magnetization data for FeSe and Pb were obtained by subtracting the magnetic contribution of the DAC measured in an empty run from the total magnetization.^{28,29,43,44} As the PTM, we mainly used Ar, which solidifies at $P=1.2$ GPa at room temperature as a soft molecular solid and is known to be a hydrostatic PTM.^{45,46} For the measurements, we adopted platelet single crystals with different thicknesses, which were ~ 20 μm or less than ~ 8 μm , while the gasket thickness was typically ~ 30 μm (40 μm)

after (before) the measurements. The thickness (t) of the platelet specimens for $t \lesssim 8$ μm was estimated by using a scanning electron microscope. Electrical resistivity of a FeSe single crystal with dimensions of $0.9 \times 0.5 \times 0.035$ mm³ was measured under pressure by using an opposed-anvil cell.⁴⁷

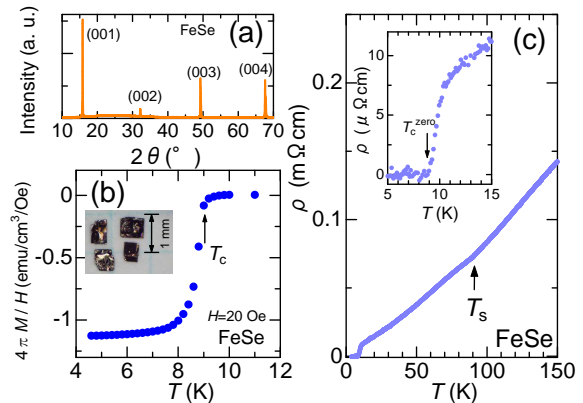


FIG. 1: (Color on line) X-ray diffraction pattern at room temperature (a), Temperature (T) dependence of zero-field-cooled DC magnetization M measured by applying a magnetic field of 20 Oe parallel to the (001) plane (b) and electrical resistivity ρ (c) for FeSe single crystals. The insets in (b) and (c) show a photographic image of typical single crystals of FeSe and an enlarged view of $\rho(T)$ at nearly zero resistivity, respectively.

Measurements were also performed using glycerin as the PTM to observe the effect of the degradation of the hydrostaticity. The $M(T)$ curves for a single crystal of FeSe with $t \sim 20$ μm at various pressures measured using glycerin as the PTM are shown in Fig. 2(a). The curve at ambient pressure shows a sharp decrease below $T_c^{\text{dia}} \sim 9$ K, and T_c^{dia} increases with increasing pressure up to ~ 25 K at 5.1 GPa. However, above the pressure, T_c^{dia} decreases and the diamagnetic amplitude decreases rapidly. The pressure evolution of $M(T)$ suggests the disappearance of superconductivity above 5–6 GPa. Figure 2(b) shows the $\rho(T)$ curves measured using glycerin at various pressures. In Fig. 2(b), the $\rho(T)$ curve at 2.0 GPa exhibits a maximum at $T_c^{\text{onset}} \sim 25$ K and a sharp decrease showing zero-resistivity below $T_c^{\text{zero}} \sim 15$ K. T_c^{zero} begins to decrease above 4.6 GPa and reaches 5 K at 6.4 GPa, while T_c^{onset} is ~ 37 K at 6.4 GPa, indicating a significant broadening of the superconducting transition. The AFM transition temperature T_m on the $\rho(T)$ curves is determined in a similar manner as in the literature.³³ These results are summarized in Fig. 2(c), where the transition temperatures are plotted as a function of pressure together with the phase boundary lines (broken lines) obtained from the measurements under hydrostatic pressure.³³ Here, both T_c^{zero} and T_c^{dia} suddenly drop above ~ 5 GPa, thereby deviating from the broken line.

The disappearance of the superconductivity above ~ 5 GPa seen in Fig. 2(a)-2(c) appears to correspond

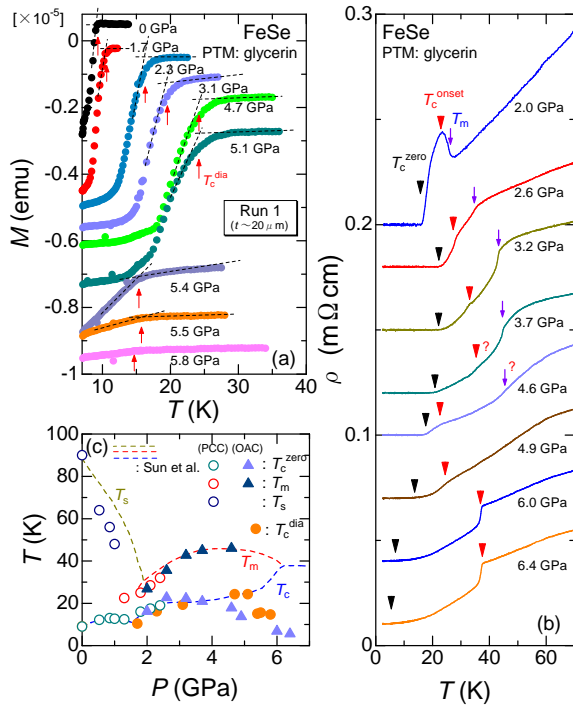


FIG. 2: (Color on line) Temperature dependence of zero-field-cooled DC magnetization M in a magnetic field of 20 Oe (a) and electrical resistivity ρ (b) at various pressures using glycerin as the PTM for FeSe. The data are intentionally shifted along the longitudinal axis for clarity. (c) Plots of diamagnetic onset (T_c^{dia}), zero-resistive (T_c^{zero}), nematic transition (T_s) and AFM transition temperatures (T_m). The data of T_c^{zero} , T_m and T_s obtained using a piston cylinder cell (PCC) in a previous study⁴¹ are also plotted, in addition to those obtained using an opposed anvil cell (OAC). The broken lines were reproduced from the literature.³³

to the solidification of glycerin above 5 GPa at room temperature,⁴⁸ which induces a nearly uniaxial compression perpendicular to the (001) plane. It should be noted that the disappearance has never been observed by applying a uniaxial stress in the [101] direction by using NaCl as the PTM, as in the previous study.²⁹ Thus, uniaxial stress, especially along the [001] direction is likely to be responsible for the disappearance of the superconductivity. $M(T)$ curves of FeSe at various pressures for FeSe with $t \sim 20 \mu\text{m}$ and $t \sim 8 \mu\text{m}$ using Ar as the PTM, are shown in Figs. 3(a) and 3(b), respectively. Fig. 3(a) shows that T_c^{dia} exhibits a local maximum at 0.82 GPa but shows a rapid increase above 1.5 GPa, reaching $T_c^{\text{dia}} \sim 30$ K at 6.7 GPa. Above 6.9 GPa, the amplitude of the diamagnetic response decreases steeply and $M(T)$ finally almost stabilizes at 7.6 GPa. In contrast, the $M(T)$ curves for $t \sim 8 \mu\text{m}$ in Fig. 3(b) indicate that T_c^{dia} exhibits a similar variation with pressure compared with that for $t \sim 20 \mu\text{m}$ up to 6.7 GPa; however, the amplitude of the diamagnetic response appears not to be reduced even above 7.0 GPa, yielding $T_c^{\text{dia}} \sim 37$ K above 7.6 GPa. To clarify the pressure evolution of the su-

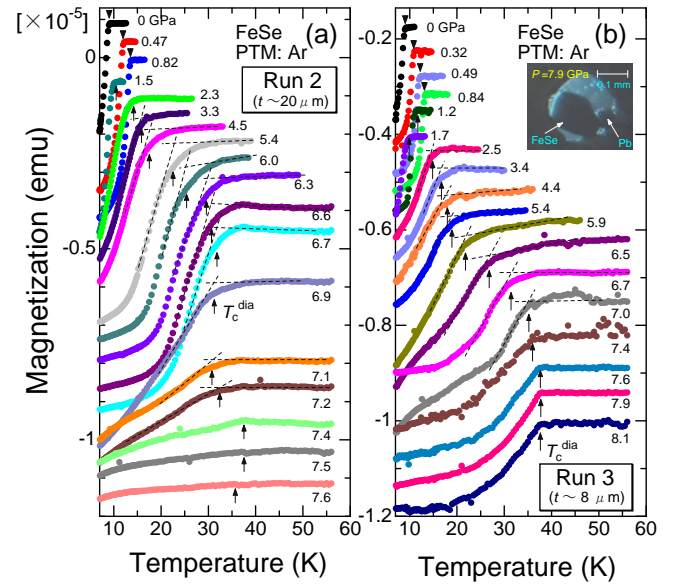


FIG. 3: (Color on line) Temperature dependence of zero-field-cooled DC magnetization for FeSe in a magnetic field of 20 Oe under various pressures using Ar as the PTM for a sample with thickness $t \sim 20 \mu\text{m}$ (a) and $\sim 8 \mu\text{m}$ (b). The data were intentionally shifted along the longitudinal axis for clarity. The inset in (b) shows the sample assembly for Run 3 at $P=7.9$ GPa.

perconducting volume fraction, we estimated it from the amplitude of the diamagnetic response as in the previous study.²⁹ The superconducting volume fraction (p) at $T=0.5T_c$ normalized by that at ambient pressure (p_0), as a function of pressure for $t \sim 20 \mu\text{m}$ and $t \sim 8 \mu\text{m}$, is plotted in Fig. 4(a) and 4(b), respectively. We excluded the contribution of Pb to the amplitude of the magnetic response to enable us to precisely estimate $p(0.5T_c)/p_0(0.5T_c)$ at low pressures. In Fig. 4(a), $p(0.5T_c)/p_0(0.5T_c)$ for $t \sim 20 \mu\text{m}$ shows an abrupt decrease to zero above ~ 5 GPa when glycerin was used as the PTM, whereas a sharp decrease was observed at pressures above ~ 7 GPa when Ar was used, indicating the disappearance of the superconductivity. The pressure variations are qualitatively similar to that of $1-p_{\text{OR2}}$, where p_{OR2} is the phase fraction of the ortho II phase and is evaluated by the relative intensity of Bragg reflections for the ortho II and tetragonal phases in the XRD measurements under pressure using He as the PTM.³⁸ This suggests that the origin of the disappearance of the superconductivity is due to the appearance of the ortho II phase. In contrast, $p(0.5T_c)/p_0(0.5T_c)$ for $t \sim 8 \mu\text{m}$ in Fig. 4(b) remains ~ 0.9 even above 7 GPa. To verify the reproducibility, the measurements were also performed using a single crystal of another batch with $t \sim 5 \mu\text{m}$ (Run 4). The results are shown in Fig. 4(b). It is confirmed that $p(0.5T_c)/p_0(0.5T_c)$ for $t \sim 5 \mu\text{m}$ remains more than 0.7 above 7 GPa. We can also observe a common tendency that $p(0.5T_c)/p_0(0.5T_c)$ is slightly reduced between $1.5 \lesssim P \lesssim 6.0$ GPa. This behavior is probably the result of the coexistence of the AFM and superconducting

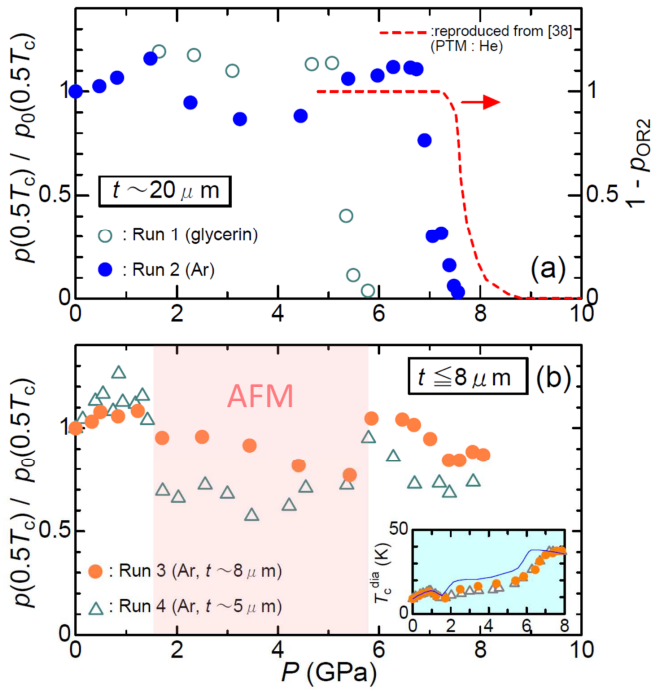


FIG. 4: (Color on line) (a) Superconducting volume fraction (p) at $T=0.5T_c$ normalized to that at ambient pressure (p_0) plotted versus pressure for FeSe single crystals with thickness $t \sim 20 \mu\text{m}$. The broken line indicates the pressure variation of $1-p_{\text{OR2}}$, where p_{OR2} is the phase fraction of the ortho II phase reproduced from the literature³⁸. (b) $p(0.5T_c)/p_0(0.5T_c)$ plotted as a function of pressure for $t \lesssim 8 \mu\text{m}$. Inset: T_c^{dia} versus pressure for specimens with $t \lesssim 8 \mu\text{m}$. The T_c-P curve determined mainly from the zero-resistive temperature by using a CAA³³ is shown as a solid line.

phases and is regarded as an evidence of the appearance of the AFM phase in the pressure region. Nonetheless, $p(0.5T_c)/p_0(0.5T_c)$ possibly reflects the broadening of the superconducting transition due to the co-existing AFM phase rather than the reduction of the superconducting volume fraction. A similar weakening of the diamagnetic shielding in the pressure region where the AFM dome appears has been observed for $\text{FeSe}_{1-x}\text{S}_x$.⁴⁹ In Figs. 4(a) and 4(b), a small increase is seen in $p(0.5T_c)/p_0(0.5T_c)$ for $0 \lesssim P \lesssim 1$ GPa. This is probably attributable to an initial shrinkage in the thickness of the single crystal, which leads to an increase in the demagnetization coefficient. The inset in Fig. 4(b) shows the pressure variations of T_c^{dia} for $t \lesssim 8 \mu\text{m}$. The $T_c^{\text{dia}}-P$ curves are qualitatively similar to the T_c-P curve determined mainly from the zero-resistive temperature by using a CAA.³³

We should note that He was used as the PTM in the previous observation of the ortho II phase by the XRD measurements above 8 GPa at room temperature.^{37,38} Based on the facts, one may consider that the ortho II phase has been induced under hydrostatic pressure, because He is generally known not to solidify up to ~ 12 GPa at room temperature.⁵⁰ However, to explain the disappearance and survival of the superconductivity, we

propose a possible scenario, in which the ortho II phase appears owing to the degradation of the hydrostaticity of the pressure for $t \sim 20 \mu\text{m}$, while the ortho II phase does not appear for $t \lesssim 8 \mu\text{m}$ because of the improvement in the hydrostaticity resulting from the decrease in the thickness of the crystal. The results for $t \lesssim 8 \mu\text{m}$ are similar to those obtained in the measurements using a CAA, which generates the perfect hydrostatic pressure by three-axis compression. Indeed, it has been shown in XRD measurements of Au using a DAC with He that the increase in the uniaxial stress component above 30 GPa tends to be suppressed as the height of the sample decreases along the load direction.⁵¹ In addition, we failed to detect any sign of the disappearance of the superconductivity using Ar as the PTM in the previous observation for a single crystal with dimensions of $\sim 0.1 \times 0.1 \times 0.02 \text{ mm}^3$ where the (101) plane is exposed on the surface.²⁹ This suggests that the disappearance is induced by a uniaxial component of the compression along a specific direction [001]. This conclusion is also supported by the results shown in Figs. 2(a)-2(c), where solid-state compression along the [001] direction accelerates the transformation to the ortho II phase. In fact, it was shown in a previous study that a large shrinkage along the c-axis in the crystal structure is accompanied by the transition to the ortho II phase, yielding a volume reduction of 11% at 300 K.³⁷ This suggests that a uniaxial stress along [001] direction could be important for the occurrence of the transition. Thus, the above-mentioned scenario is most likely, although it is unclear how uniaxial stress can be generated for $P < 12$ GPa at room temperature by using He as PTM. The relationship among the three phases on the $T-P$ phase diagram still remains to be fully understood not only in pure-FeSe, but also in S-doped⁵² and Te-doped FeSe,⁵³ as is suggested by the recent study reporting the coexistence of superconductivity and magnetic order on a tetragonal lattice above 6 GPa.³⁸ Further investigations at high pressure are necessary in future studies. However, special attention should be given to the hydrostaticity of the pressure, which greatly affects the crystal structure of the single crystal specimen with the (001) surface.

In summary, by conducting the DC magnetization measurements, we successfully observed the disappearance of the superconductivity in FeSe owing to the appearance of the ortho II phase. In addition, the survival of the superconductivity owing to the absence of the ortho II phase was also observed using platelet single crystal specimens with different thicknesses. It is inferred from the results using both Ar and glycerin for the specimens with $t \sim 20 \mu\text{m}$ that uniaxial stress along the [001] direction is essential to realize the ortho II phase. The superconducting volume fraction for specimens with $t \lesssim 8 \mu\text{m}$ was found to show no sudden decrease at high pressure. This is consistent with the result observed in the measurements under hydrostatic pressure using a CAA³³, such that the hydrostaticity can be improved by reducing the thickness of the specimens in our measurements. In

conclusion, we emphasize that the thickness of the sample can be important for the hydrostaticity in the measurements using a DAC, even though a hydrostatic PTM is used.

Acknowledgments

This work was supported by JSPS KAKENHI (Grant Number JP18K03516). The authors thank T. Mat-

sumoto, D. Morii, T. Ohyama, A. Nishiyama and T. Sueyasu for technical assistance.

-
- ¹ Y. Kamihara, T. Watanabe, M. Hirano, and H. Hosono, *J. Am. Chem. Soc.* **130**, 3296 (2008).
- ² M. Rotter, M. Tegel and D. Johrendt, *Phys. Rev. Lett.* **101**, 107006 (2008).
- ³ N. Ni, M. E. Tillman, J.-Q. Yan, A. Kracher, S. T. Hannahs, S. L. Bud'ko, and P. C. Canfield, *Phys. Rev. B* **78**, 214515 (2008).
- ⁴ A. S. Sefat, R. Jin, M. A. McGuire, B. C. Sales, D. J. Singh and D. Mandrus, *Phys. Rev. Lett.* **101**, 117004 (2008).
- ⁵ S. Kasahara, H. J. Shi, K. Hashimoto, S. Tonegawa, Y. Mizukami, T. Shibauchi, K. Sugimoto, T. Fukuda, T. Terashima, A. H. Nevidomskyy and Y. Matsuda, *Nature* **486**, 382 (2012).
- ⁶ M. S. Torikachvili, S. L. Bud'ko, N. Ni, and P. C. Canfield, *Phys. Rev. B* **78**, 104527 (2008).
- ⁷ F. Ishikawa, N. Eguchi, M. Kodama, K. Fujimaki, M. Einaga, A. Ohmura, A. Nakayama, A. Mitsuda, and Y. Yamada, *Phys. Rev. B* **79**, 172506 (2009).
- ⁸ E. Colombier, S. L. Bud'ko, N. Ni, and P. C. Canfield, *Phys. Rev. B* **79**, 224518 (2009).
- ⁹ T. Yamazaki, N. Takeshita, R. Kobayashi, H. Fukazawa, Y. Kohori, K. Kihou, C.-H. Lee, H. Kito, A. Iyo, and H. Eisaki, *Phys. Rev. B* **81**, 224511 (2010).
- ¹⁰ H. Kotegawa, H. Sugawara, and H. Tou, *J. Phys. Soc. Jpn.* **78**, 013709 (2009).
- ¹¹ K. Matsubayashi, N. Katayama, K. Ohgushi, A. Yamada, K. Munakata, T. Matsumoto, and Y. Uwatoko, *J. Phys. Soc. Jpn.* **78**, 073706 (2009).
- ¹² T. Terashima, M. Kimata, H. Satsukawa, A. Harada, K. Hazama, S. Uji, H. S. Suzuki, T. Matsumoto, and K. Murata, *J. Phys. Soc. Jpn.* **78**, 083701 (2009).
- ¹³ H. Luetkens, H.-H. Klauss, M. Kraken, F. J. Litterst, T. Dellmann, R. Klingeler, C. Hess, R. Khasanov, A. Amato, C. Baines, M. Kosmala, O. J. Schumann, M. Braden, J. Hamann-Borrero, N. Leps, A. Kondrat, G. Behr, J. Werner, and B. Büchner, *Nat. Mater.* **8**, 305 (2009).
- ¹⁴ D. R. Parker, M. J. P. Smith, T. Lancaster, A. J. Steele, I. Franke, P. J. Baker, F. L. Pratt, M. J. Pitcher, S. J. Blundell, and S. J. Clarke, *Phys. Rev. Lett.* **104**, 057007 (2010).
- ¹⁵ A. F. Wang, X. G. Luo, Y. J. Yan, J. J. Ying, Z. J. Xiang, G. J. Ye, P. Cheng, Z. Y. Li, W. J. Hu, and X. H. Chen, *Phys. Rev. B* **85**, 224521 (2012).
- ¹⁶ A. F. Wang, J. J. Lin, P. Cheng, G. J. Ye, F. Chen, J. Q. Ma, X. F. Lu, B. Lei, X. G. Luo, and X. H. Chen, *Phys. Rev. B* **88**, 094516 (2013).
- ¹⁷ K. Ueshima, F. Han, X. Zhu, H. H. Wen, S. Kawasaki, and G. -q. Zheng, *Phys. Rev. B* **89**, 184506 (2014).
- ¹⁸ S. Hohenstein, F. Hummel, Z. Guguchia, S. Kamusell, N. Barbero, H. Ogino, Z. Shermadini, R. Khasanov, A. Amato, T. Shiroka, H.-H. Klauss, E. Morenzoni, D. Johrendt, and H. Luetkens, arXiv:1911.04319.
- ¹⁹ S. Iimura, S. Matuishi, H. Sato, T. Hanna, Y. Muraba, S. W. Kim, J. E. Kim, M. Takata, and H. Hosono, *Nat. Commun.* **3**, 943 (2012).
- ²⁰ M. Hiraishi, S. Iimura, K. M. Kojima, J. Yamaura, H. Hiraka, K. Ikeda, P. Miao, Y. Ishikawa, S. Torii, M. Miyazaki, I. Yamauchi, A. Koda, K. Ishii, M. Yoshida, J. Mizuki, R. Kadono, R. Kumai, T. Kamiyama, T. Otomo, Y. Murakami, S. Matsuishi, and H. Hosono, *Nat. Phys.* **10**, 300 (2014).
- ²¹ C. Wang, S. Jiang, Q. Tao, Z. Ren, Y. Li, L. Li, C. Feng, J. Dai, G. Cao, and Z. Xu, *Europhys. Lett.* **86**, 47002 (2009).
- ²² K. T. Lai, A. Takemori, S. Miyasaka, F. Engetsu, H. Mukuda, and S. Tajima, submitted to *Phys. Rev. B* **90**, 064504 (2014).
- ²³ H. Mukuda, F. Engetsu, T. Shiota, K. T. Lai, M. Yashima, Y. Kitaoka, S. Miyasaka, and S. Tajima, *J. Phys. Soc. Jpn* **83**, 083702 (2014).
- ²⁴ S. Masaki, H. Kotegawa, Y. Hara, H. Tou, K. Murata, Y. Mizuguchi, and Y. Takano, *J. Phys. Soc. Jpn.* **78**, 063704 (2009).
- ²⁵ S. Medvedev, T. M. McQueen, I. A. Troyan, T. Palasyuk, M. I. Erements, R. J. Cava, S. Naghavi, F. Casper, V. Ksenofontov, G. Wortmann, and C. Felser, *Nat. Mater.* **8**, 630 (2009).
- ²⁶ S. Margadonna, Y. Takabayashi, Y. Ohishi, Y. Mizuguchi, Y. Takano, T. Kagayama, T. Nakagawa, M. Takata, and K. Prassides, *Phys. Rev. B* **80**, 064506 (2009).
- ²⁷ D. Braithwaite, B. Salce, G. Lapertot, F. Bourdarot, C. Marin, D. Aoki, and M. Hanfland, *J. Phys.: Condens. Matter* **21**, 232202 (2009).
- ²⁸ K. Miyoshi, Y. Takaichi, E. Mutou, K. Fujiwara, and J. Takeuchi, *J. Phys. Soc. Jpn.* **78**, 093703 (2009).
- ²⁹ K. Miyoshi, K. Morishita, E. Mutou, M. Kondo, O. Seida, K. Fujiwara, J. Takeuchi, and S. Nishigori, *J. Phys. Soc. Jpn.* **83**, 013702 (2014).
- ³⁰ A. E. Böhmer, F. Hardy, F. Eilers, D. Ernst, P. Adelman, P. Schweiss, T. Wolf, and C. Meingast, *Phys. Rev. B* **87**, 180505(R) (2013).
- ³¹ A. E. Böhmer, V. Taufour, W. E. Straszheim, T. Wolf, and P. C. Canfield, *Phys. Rev. B* **94**, 024526 (2016).
- ³² T. Terashima, N. Kikugawa, S. Kasahara, T. Watashige, T. Shibauchi, Y. Matsuda, T. Wolf, A. E. Böhmer, F. Hardy, C. Meingast, H. v. Löhneysen, and S. Uji, *J. Phys. Soc. Jpn.* **84**, 063701 (2015).

- ³³ J. P. Sun, K. Matsuura, G. Z. Ye, Y. Mizukami, M. Shimozawa, K. Matsubayashi, M. Yamashita, T. Watashige, S. Kasahara, Y. Matsuda, J.-Q. Yan, B. C. Sales, Y. Uwatoko, J.-G. Cheng and T. Shibauchi, *Nat. Commun.* **7**, 12146 (2016).
- ³⁴ P. S. Wang, S. S. Sun, Y. Cui, W. H. Song, T. R. Li, R. Yu, H. Lei, and W. Yu, *Phys. Rev. Lett.* **117**, 237001 (2016).
- ³⁵ R. Khasanov, Z. Guguchia, A. Amato, E. Morenzoni, X. Dong, F. Zhou, and Z. Zhao *Phys. Rev. B* **95**, 180504(R) (2017).
- ³⁶ K. Kothapalli, A. E. Böhmer, W.T. Jayasekara, B. G. Ueland, P. Das, A. Sapkota, V. Taufour, Y. Xiao, E. Alp, S. L. Bud'ko, P. C. Canfield, A. Kreyssig, and A. I. Goldman, *Nat. Commun.* **7**, 12728 (2016).
- ³⁷ V. Svitlyk, M. Raba, V. Dmitriev, P. Rodiere, P. Toulemonde, D. Chernyshov, and M. Mezouar *Phys. Rev. B* **96**, 014520 (2017).
- ³⁸ A. E. Böhmer, K. Kothapalli, W. T. Jayasekara, J. M. Wilde, B. Li, A. Sapkota, B. G. Ueland, P. Das, Y. Xiao, W. Bi, J. Zhao, E. E. Alp, S. L. Bud'ko, P. C. Canfield, A. I. Goldman, and A. Kreyssig, *Phys. Rev. B* **100**, 064515 (2018).
- ³⁹ B. W. Lebert, V. Baledent, P. Toulemonde, J. M. Ablett, and J.-P. Rueff, *Phys. Rev. B* **96**, 180503(R) (2018).
- ⁴⁰ R. S. Kumar, Y. Zhang, S. Sinogeikin, Y. Xiao, S. Kumar, P. Chow, A. L. Cornelius, and C. Chen, *J. Phys. Chem. B* **114**, 12597 (2010).
- ⁴¹ K. Miyoshi, A. Shiota, S. Kato, S. Yamamoto, K. Fujiwara and S. Nishigori, *JPS Conf. Proc.* **30**, 011068 (2020).
- ⁴² M. Mito, M. Hitaka, T. Kawae, K. Takeda, T. Kitai, and N. Toyoshima, *Jpn. J. Appl. Phys.* **40**, 6641 (2001).
- ⁴³ K. Miyoshi, Y. Takaichi, Y. Takamatsu, M. Miura, and J. Takeuchi, *J. Phys. Soc. Jpn.* **77**, 043704 (2008).
- ⁴⁴ K. Miyoshi, E. Kojima, S. Ogawa, Y. Shimojo, and J. Takeuchi, *Phys. Rev. B* **87**, 235111 (2013).
- ⁴⁵ L. W. Finger, R. M. Hazen, G. Zou, H. K. Mao, and P. M. Bell, *Appl. Phys. Lett.* **39**, 892 (1981).
- ⁴⁶ N. Tateiwa and Y. Haga, *Rev. Sci. Instrum.* **80**, 123901 (2009).
- ⁴⁷ K. Kitagawa, H. Gotou, T. Yagi, A. Yamada, T. Matsumoto, Y. Uwatoko, and M. Takigawa, *J. Phys. Soc. Jpn.* **79**, 024001 (2010).
- ⁴⁸ A. Drozd-Rzoska, S. J. Rzoska, M. Paluch, A. R. Imre, and C. M. Roland, *J. Chem. Phys.* **126**, 164504 (2007).
- ⁴⁹ K. Y. Yip, Y. C. Chan, Q. Niu, K. Matsuura, Y. Mizukami, S. Kasahara, Y. Matsuda, T. Shibauchi, and Swee K. Goh, *Phys. Rev. B* **96**, 020502(R) (2017).
- ⁵⁰ P. M. Bell and H. K. Mao, *Carnegie Inst. Washington Yearbook* **80**, 404 (1981).
- ⁵¹ K. Takemura and A. Dewaele, *Phys. Rev. B* **78**, 104119 (2008).
- ⁵² K. Matsuura, Y. Mizukami, Y. Arai, Y. Sugimura, N. Maejima, A. Machida, T. Watanuki, T. Fukuda, T. Yajima, Z. Hiroi, K. Y. Yip, Y.C. Chan, Q. Niu, S. Hosoi, K. Ishida, K. Mukasa, S. Kasahara, J.-G. Cheng, S.K. Goh, Y. Matsuda, Y. Uwatoko and T. Shibauchi, *Nat. Commun.* **8**, 1143 (2017).
- ⁵³ K. Mukasa, K. Matsuura, M. Qiu, M. Saito, Y. Sugimura, K. Ishida, M. Otani, Y. Onishi, Y. Mizukami, K. Hashimoto, J. Gouchi, R. Kumai, Y. Uwatoko and T. Shibauchi *Nat. Commun.* **12**, 381 (2021).